Journal of Anatomy

J. Anat. (2011) **218**, pp263–270 doi: 10.1111/j.1469-7580.2010.01332.x

Innervation patterns of PGP 9.5-positive nerve fibers within the human lumbar vertebra

Jeannie F. Bailey,[1] Ellen Liebenberg,[1] Sean Degmetich[1,2] and Jeffrey C. Lotz[1]

[1]*Orthopaedic Bioengineering Laboratory, University of California, San Francisco, CA, USA*
[2]*Relievant Medsystems, Inc., Redwood City, CA, USA*

Abstract

Intervertebral disc injury or degeneration is a common cause of low back pain, and yet the specific source of pain remains ambiguous in many cases. Previous research indicates that the central vertebral endplate is highly innervated and can elicit pain responses to pressure. In effort to trace the origin of nerves located at the endplate, we used protein gene product 9.5 (PGP 9.5) to stain neurofibers and then quantified the spatial pattern of nerve distribution within a human L4 lumbar vertebra. The majority of nerves were adjacent to blood vessel walls, and consequently the nerve distribution closely resembled previously established vascularity patterns. We observed that the majority of nerves enter the vertebral body posteriorly, via the basivertebral foramen, and cluster in the vertebral center. These nerves follow the course of the nutrient artery, which enters the vertebral body through the basivertebral foramen, then branches toward the superior and inferior endplates. Our observations support the notion that nerves found at the central endplate could originate from sinuvertebral nerves accompanying the nutrient artery into the vertebral body. We also stained neighboring histological sections with calcitonin gene-related protein and noted significant co-localization with PGP 9.5, substantiating a nociceptive role for the nerves constituting our distribution pattern.

Key words: basivertebral nerve; endplate; innervation; low back pain; vertebral body.

Introduction

The intervertebral disc forms an avascular, fibrocartilaginous joint between adjacent vertebral bodies. It is composed of three major sub-tissues: the gelatinous nucleus pulposus, the fibrous annulus fibrosus, and cartilaginous endplate. The nucleus pulposus is centrally located, composed primarily of proteoglycans and water, and serves as the osmotic mechanism that generates pressure and volume to support spinal forces. The annulus fibrosus is firmly attached to the vertebral edges and surrounds the nucleus pulposus. It serves both as a ligament to guide intervertebral movement and as a barrier to contain nuclear swelling, thereby facilitating disc pressurization. The cartilaginous endplate is a thin (0.1–1.6 mm) hyaline cartilage layer that separates the nucleus from the adjacent vertebra and is supported by porous subchondral bone. It serves as a semipermeable membrane to allow diffusive communication between disc nuclear cells and vertebral vasculature, as well as to prevent large molecular weight proteoglycans from leaving the nuclear space.

Intervertebral disc injury or degeneration is a common cause of low back pain, and yet the specific pain source is unknown for many patients. The disc in its healthy state is avascular and aneural, except for sparse nerves and vessels in the peripheral annulus (Malinsky, 1959; Bogduk et al. 1981; Humzah & Soames, 1988). By contrast, the adjacent vertebral bodies are highly vascularized and innervated, with vertebral capillaries providing the principal nutritive support for disc nucleus cells (Antonacci et al. 1998; van Dieen et al. 1999). With disc degeneration, the vertebral endplate exhibits increased sensory and sympathetic innervation (Brown et al. 1997; Freemont et al. 2002). Endplate nerves are prototypical pain fibers that display nociceptor markers such as the neurotransmitter substance P and high affinity nerve growth factor receptor trk-A (Freemont et al. 2002). The density of endplate innervation can be comparable to that of the peripheral annulus, suggesting that the endplate is an important source of discogenic pain (Fagan et al. 2003). This notion is supported by imaging studies correlating endplate abnormalities with pain (Weishaupt et al. 2001), surgical reports demonstrating that the endplate is painful when touched (Kuslich et al. 1991), and

Correspondence
Jeffrey C. Lotz, Orthopaedic Bioengineering Laboratory, University of California, 533 Parnassus Ave, 4th Floor, U454, San Francisco, CA 94143-0514, USA. E: lotzj@orthosurg.ucsf.edu

Accepted for publication *27 November 2010*
Article published online *12 January 2011*

clinical data indicating that back pain is ameliorated after disrupting vertebral nerves during vertebroplasty (Niv et al. 2003).

Despite its potential relevance to spinal pain, the source and pattern of vertebral innervation is not well described. As early as 1963, Sherman (1963) observed a 'large solitary nerve trunk' entering the vertebral body via a bony tunnel in the posterior cortex, the basivertebral foramen (BVF). More recently, Antonacci et al. (1997) analyzed a large sample of human vertebra and consistently demonstrated the presence of neurovascular bundles within the BVF, coining the phrase 'basivertebral nerves'. Subsequently, these interosseus nerves were observed to be more prevalent in regions of bone microdamage (Antonacci et al. 1997, 2002). Although these studies have confirmed the presence of nerves in the vertebral body using various histological neural markers, they have not revealed innervation pathways that may link endplate nociceptors to the basivertebral nerve trunk. The goal of this current study was to quantify the spatial pattern of nerve density within lumbar vertebra. We demonstrate that central endplate nociceptors arise from nerves entering the posterior vertebral body through the BVF.

Materials and methods

Preparation and staining

One L4 vertebra was isolated from the lumbar spine of a 60-year-old male within 72 h *post-mortem* (Willed Body Program, UC San Francisco). Dissection involved careful removal of the surrounding musculature, adjacent vertebral discs and posterior vertebral arch. The posterior longitudinal ligament was left intact to insure that nerves were undisturbed within the BVF.

To facilitate adequate processing for histologic analyses, the vertebral body was then cut across the coronal plane into five separate, parallel slabs, each being 5–7 mm in thickness. The resulting five specimens were then fixed for 7 days in 10% neutral buffered formalin (Thermo Fisher Scientific). Specimens were decalcified with Ion Exchange Decal, a mild but rapid ion exchange decalcifier (BioCare Medical), until a radiographic endpoint test confirmed the specimens as calcium-negative. Specimens were then dehydrated in an ascending series of ethanol and cleared with Clearite 3 (Richard Allen), then infiltrated and embedded in paraffin. Each slab was further sectioned coronally on a rotary microtome at 200-μm increments. Sections (7 μm thick) were then mounted on slides and stained with one of several neuronal markers: calcitonin gene-related protein (CGRP; Sigma Aldrich), neurofilament 200 (NF200; Thermo Fisher Scientific), and protein gene product 9.5 (PGP 9.5; Serotec). Each section was counterstained with Giemsa. CGRP is a neuropeptide found in small myelinated and unmyelinated nociceptors involved in inflammatory pain. NF200 is a marker for large-diameter myelinated neurons, intermediate filaments, and A-delta fibers that report sharp pain. PGP 9.5 is a cytoplasmic ubiquitin C-terminal hydrolase present in all classes of nerves. PGP 9.5 provided the best nerve contrast and was the stain ultimately used for calculating nerve density.

Imaging and marking

A total of 34 equally spaced PGP 9.5-stained sections were selected for imaging. Images of the slides were taken under 40× total magnification (Nikon Eclipse E800) and tiled together using a motorized stage to create composites of the entire cross-sectional vertebral body (NewCAST, Visiopharm, Hørsholm, Denmark; Fig. 1A). To enhance contrast between nerves and background staining, PGP 9.5-positive nerves were marked manually in red on a separate image layer for each section (ADOBE PHOTOSHOP CS3 Extended; Fig. 1A). Attention was taken to only mark nerves residing within the trabecular region of the vertebral body. For example, large nerves were observed within the periosteum, but only nerves within the vertebral centrum were marked.

Analysis

Each image was reoriented electronically to assure proper spatial alignment of all 34 sections. The total size of each image was set to a width and height of 9642 by 5844 pixels for consistency (at a resolution of 7429.5 ppi). The background image of the immunostained section was then removed, leaving only the red nerve markings on an otherwise blank image (Fig. 1A). The resulting nerve-only images were analyzed using IMAGEJ (NIH). To generate graphs depicting the areal nerve density distribution across the entire vertebral body, each of the 34 nerve images was divided into nine equally sized (9653×648 pixels) rectangular regions of interest (ROI). The nine ROIs formed horizontal bands stacked from the inferior endplate to the superior endplate (Fig. 1B). This was done to quantify differences in nerve density moving from the mid-transverse plane of the vertebral body towards the endplates. Within each ROI, the total nerve area was measured (in mm^2) and the number of individual nerves was counted. Surface graphs of areal nerve density that included data from all 34 sections were generated using MATLAB (The MathWorks, Inc., Natick, MA, USA; Fig. 1B). The resulting graphs demonstrate the nerve distribution and frequencies from a sagittal view of the vertebral body.

In addition, the L5 vertebra from the same donor was processed similarly to confirm the nerve density patterns observed for L4. L5 was sectioned in the sagittal plan and mid-sagittal sections were used to calculate nerve density. For three mid-sagittal sections (laterally spanning 1.5 mm), we applied an 8×10 grid to the nerve images from each of the sections, creating 80 ROI to measure nerve area and count.

Results

The PGP 9.5 protocol provided a higher specificity for nerve tissue without confounding background staining and, consequently, was preferable for distinguishing nerves from surrounding tissues. Amongst clearly identified nerves there was significant co-localization of the neuronal marker, CGRP (Fig. 2).

Most nerves were observed within or adjacent to the blood vessel walls and varied widely in size. The largest blood vessels and nerves were located within the BVF, while smaller blood vessels and nerves were found closer to the

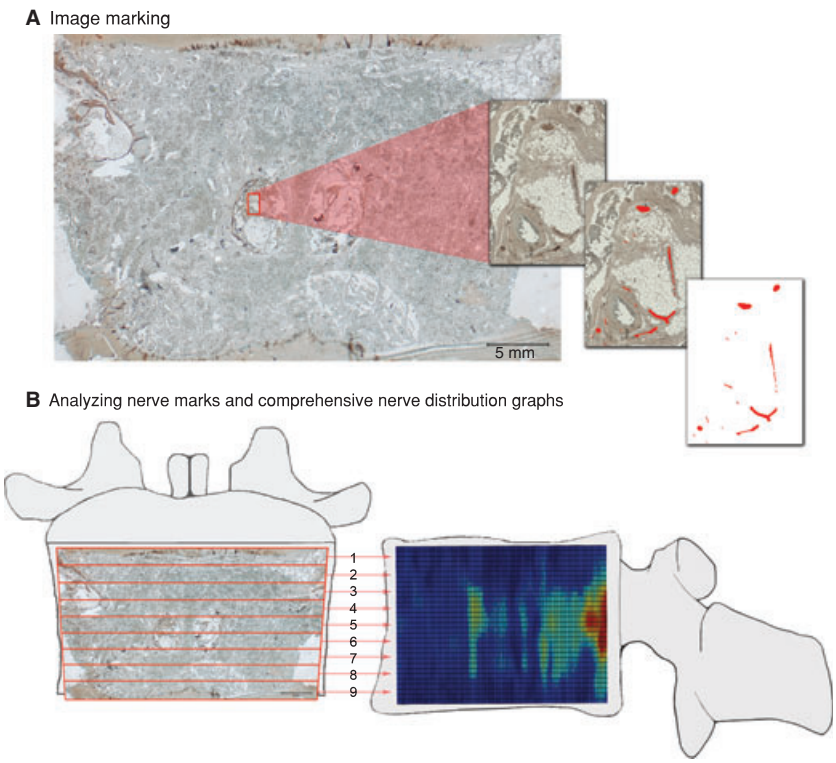

Fig. 1 (A) An image composite of an example coronal section. A small area is selected within the foramen and magnified to demonstrate the marking process first showing unmarked nerves stained dark brown with PGP9.5, then having been marked, and lastly an image of the nerves only. (B) The orientation of nine red-outlined regions of interest (ROI). The data from these nine ROI are then presented along the *y*-axis and organized for each of the 34 sections along the *x*-axis. These graphs generate a sagittal view of the nerves distribution throughout the vertebral body.

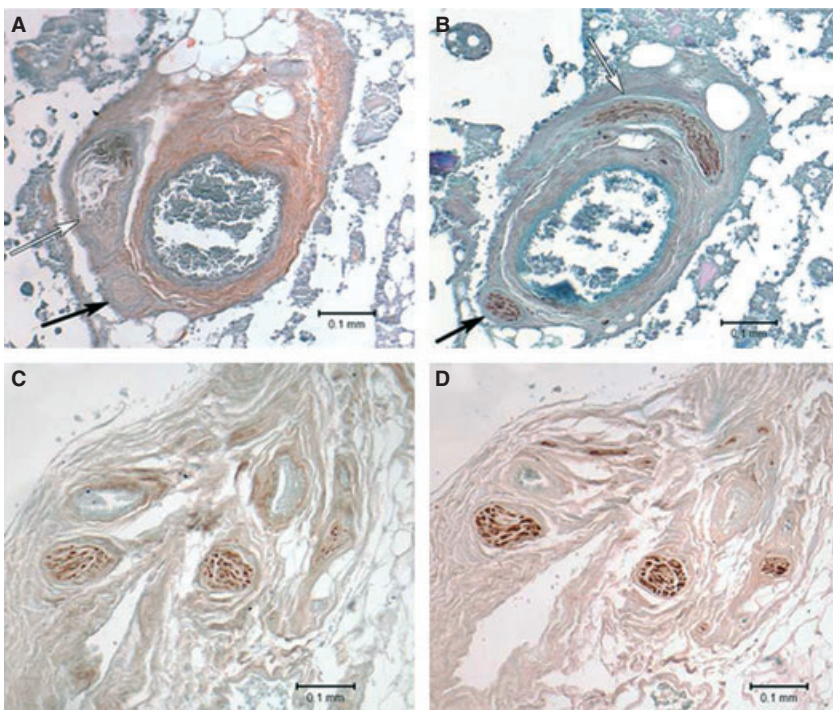

Fig. 2 (A) A blood vessel stained with calcitonin gene-related protein. (B) The same blood vessel but 5 μm away and stained with protein gene product 9.5 (PGP 9.5). (C) A blood vessel stained with NF200. (D) The same blood vessel but 9 μm away and stained with PGP 9.5.

endplates. A small number of nerves were not associated with blood vessels and were randomly distributed throughout the vertebral body (Fig. 3). The average size of nerves located within the third of the vertebral body closest to the endplates was smaller (mean = 6.37×10^{-4} mm^2, SD = 5.46×10^{-4} mm^2, range = 0.069 mm^2) than those found in the center third (mean = 7.97×10^{-4} mm^2, SD = 1.55×10^{-3} mm^2, range = 0.010 mm^2). A Student's *t*-test verified a significant difference between these two distributions ($P < 0.0001$).

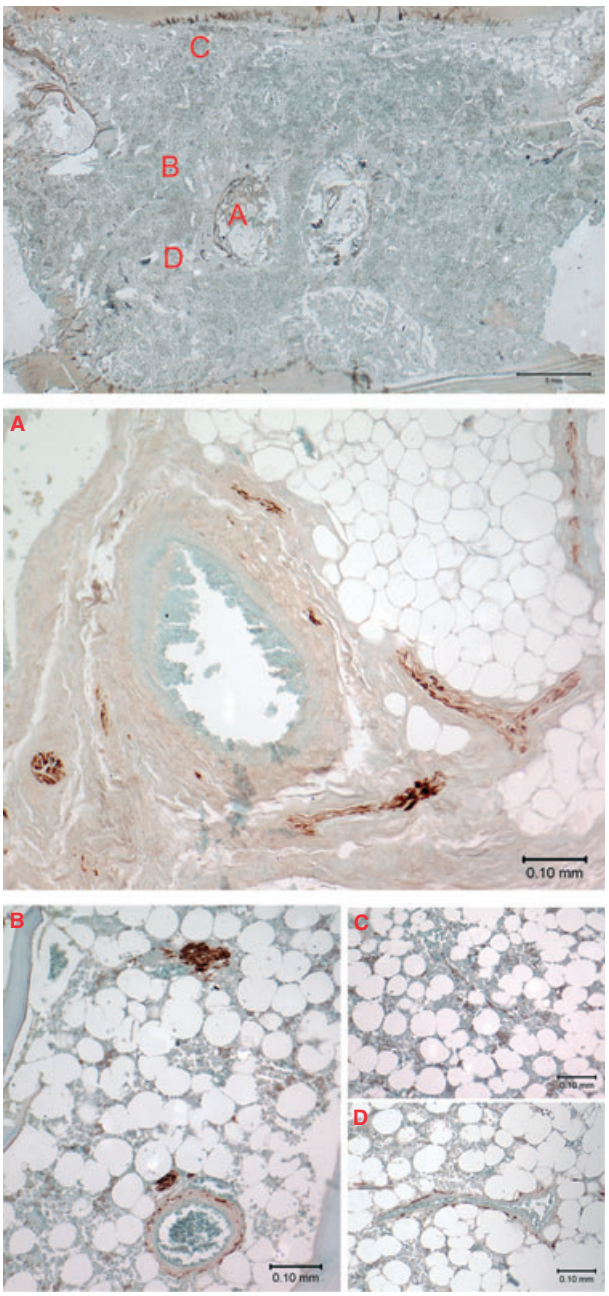

Fig. 3 Top composite image shows where the following images A through D are located along a coronal section of the posterior vertebral body. (A) The large vessels and nerves located in the basivertebral foramen. (B) A nerve unassociated with a blood vessel above and a typically innervated blood vessel below. (C) A very thin nerve moving diagonally and located near the superior endplate. (D) Another typically innervated blood vessel.

There was a strong correlation between the area and count patterns ($R^2 = 0.78$, $P < 0.0001$). The resulting L4 nerve and count graphs revealed that most vertebral nerves lie within the BVF (Fig. 4). A second nerve area peak occurred in the center of the vertebral body, near the BVF terminus. Here, the nerves form large clusters associated with a rich blood vessel network (Fig. 5). Nerve frequency decreased as it progressed towards the endplates and the small number of nerves found near the endplates were impartially distributed across the entire endplate region, with the exception of the posterior border of the endplate, which showed greater endplate innervation.

The L5 nerve area (Fig. 6) and count showed similar patterns to that from L4, with a large peak near the mid-posterior border and a second peak in the vertebral center.

Discussion

Our data demonstrate that the interior of the lumbar vertebral body is highly innervated, with the majority of nerves entering through the BVF and clustering in the center of the body. The nerves vary in shape and size (Fig. 3), and most are associated with blood vessels. The affiliation of the nerves with blood vessels is consistent with a previous histologic analysis of mouse femora showing that trabecular bone is innerved by a dense network of CGRP-positive fibers, entering alongside arteries via nutrient foramen (Mach et al. 2002). It is not surprising, therefore, that our nerve area pattern resembles that of the vertebral blood supply. Using vascular injection of radiopaque substances, early studies investigating the vascular anatomy of the vertebral body have demonstrated that after branching from the lumbar artery, the nutrient artery enters the vertebra via the BVF and courses toward the vertebral center, where it clusters (Crock & Yoshizawa, 1976; Ratcliffe, 1981). These vessels then branch in ascending and descending trajectories to supply the central endplate. Consequently, while connectivity is difficult to establish independently for nerves, their consistent association with blood vessels is indirect evidence that endplate nerves arise from the basivertebral nerve trunk. Branches of the lumbar artery have also been shown to penetrate the mid-transverse plane of the anteriolateral vertebral body and supply the vasculature of the peripheral anteriolateral vertebral body and corresponding endplates (Crock & Yoshizawa, 1976; Ratcliffe, 1981). While we observed nerves at several locations within the vertebral periosteum, we did not observe significant penetration of these nerves through the anterior or lateral cortices into the vertebral body (Figs 4 and 7).

It has been established that the nerves accompanying the nutrient artery through the BVF originate from the sinuvertebral nerves (Bogduk et al. 1981; Bogduk, 1983). The sinuvertebral nerves originate from the sympathetic trunk (Groen et al. 1990) and are found within the vertebral canal, supplying the posterior longitudinal ligament and the posterior peripheral annulus (Bogduk, 1983). Our resulting nerve distribution shows a large point of entry at the BVF and a heightened frequency of nerve along the posterior border of the vertebral body (including the endplate) and essentially none near the anteriolateral cortex. The majority of nerves we uncovered seem to penetrate from

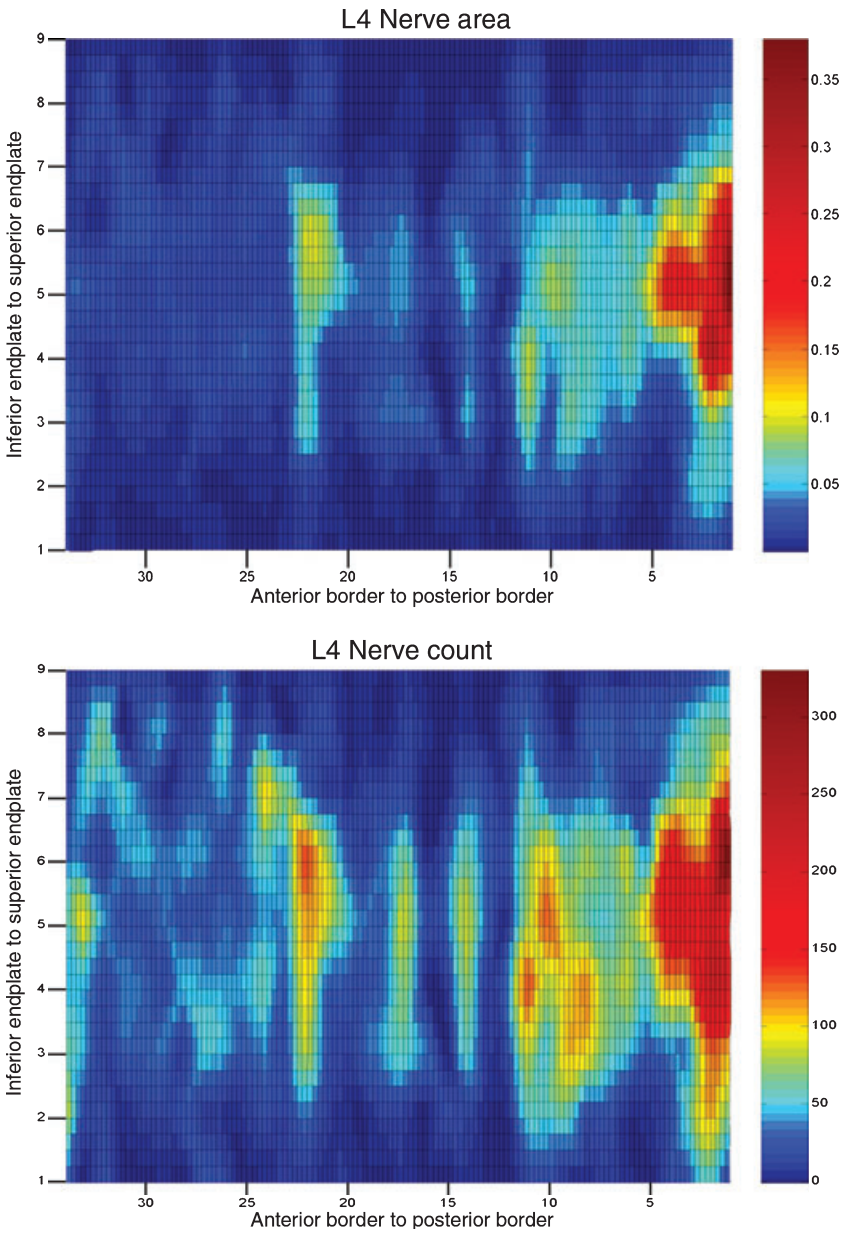

Fig. 4 For each graph, nerve data from each of the nine regions of interest (ROI) is oriented along the *y*-axis. The *x*-axis organizes the 34 sections from anterior to posterior with data from each ROI composing a complete sagittal view of the L4 interior. *L4 Nerve Area* depicts the quantity of nerve (mm^2) in each ROI among the 34 sections. *L4 Nerve Count* shows the number of individual nerves in each ROI among the 34 sections.

the posterior border and presumably originate from the sinuvertebral nerve.

The central vascularity of the vertebral body is established during fetal development, while peripheral vessels persist after adolescence (Ratcliffe, 1986). Tortuosity of the central intravertebral arteries and presence of vessels around the vertebral periphery increases with age (Ratcliffe, 1986) and is thought to be variable based on degeneration and nutrient availability. It has been demonstrated that the central arteries of the vertebral body are provided via the nutrient artery entering the BVF (Crock & Yoshizawa, 1976; Ratcliffe, 1980). The fetal ontogeny of the nutrient artery implies a consistency in its presence amongst vertebrae of all ages, whereas the peripheral vessels are acquired later in development in response to degenerative changes. The variable presence of peripheral vessels could possibly explain the lack of peripheral nerves in our L4 vertebral body.

The annular periphery is known to have small nerves and vessels that could contribute to innervating the adjacent vertebral endplate rim. These arise from the metaphyseal arteries coursing along the lateral vertebral column and house nerve branches from the gray ramus communicans, separate from the sinuvertebral nerves (Bogduk et al. 1981). These innervated metaphyseal arteries are also reported to inhabit the outer third of the vertebral body. Yet, there remains uncertainty as to the origins of the peripheral vessels due to the difficulty in distinguishing metaphyseal arteries from coiled nutrient arteries occupying the

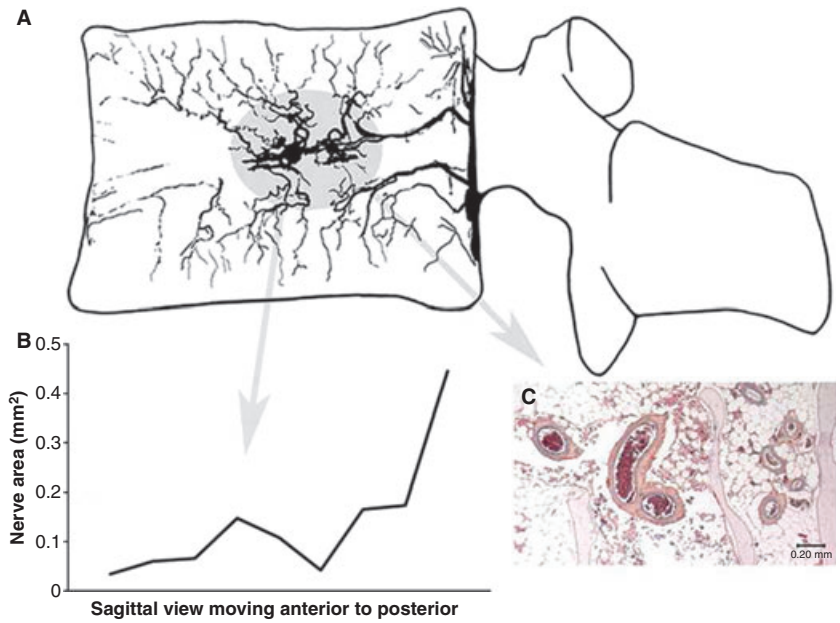

Fig. 5 (A) An adaptation from Crock & Yoshizawa (1976), demonstrating the vascularity seen across a sagittal cross-section of a lumbar vertebra. (B) A nerve density graph from our L4 vertebra correlating the vascular arterial clusters from Crock & Yoshizawa (1976) to high density nerve regions in the center portion of the nerve density graph. (C) An image of a cluster of innervated vessels from a coronal section taken of the center of the vertebral body, verifying the presence of the central arterial clusters within the L4 vertebra.

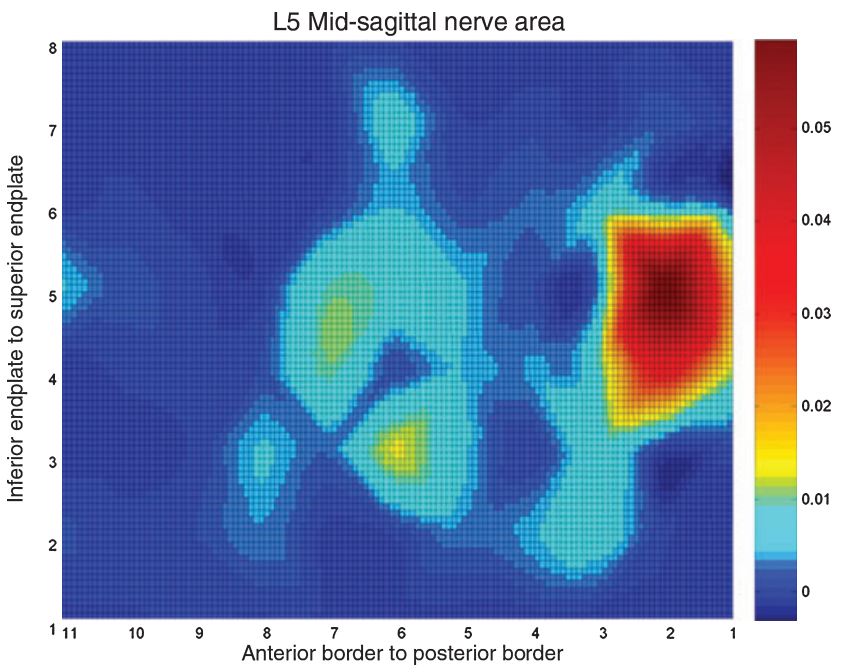

Fig. 6 *L5 Mid-Sagittal Nerve Area* is an average of nerve area (mm^2) results amongst three mid-sagittal sections from an L5 vertebral body. The sagittal sections demonstrate a similar pattern of nerves, mainly residing in the basivertebral foramen and center of the vertebral body.

vertebral centrum (Ratcliffe, 1986). Innervated arteries were present in the mid-lateral regions of our L4 vertebral body, but their nerve quantity was insignificant in comparison with that of the nutrient and central arteries (Fig. 7) and we cannot distinguish their origin. Therefore, the small number of nerves found near the central endplate must originate from the large nerves accompanying the nutrient artery through the BVF. The nerves found within posterior border of the endplate can be attributed to the close proximity of the posterior longitudinal ligament and, therefore, originate from sinuvertebral nerves. The sparse nerves found around the anteriolateral periphery of the endplate could be the origin of nerves belonging to indistinguishable central arteries located in the periphery or metaphyseal arteries around either the peripheral vertebral body or outer annulus.

Despite the common belief that bone pain arises from the periosteum, our data demonstrates that the vertebral body itself contains nerves and can be a source of pain. Consistent with past reports, we show that the basivertebral nerves are CGRP-positive, substantiating their role in nociception (Fagan et al. 2003). In support of this, others have

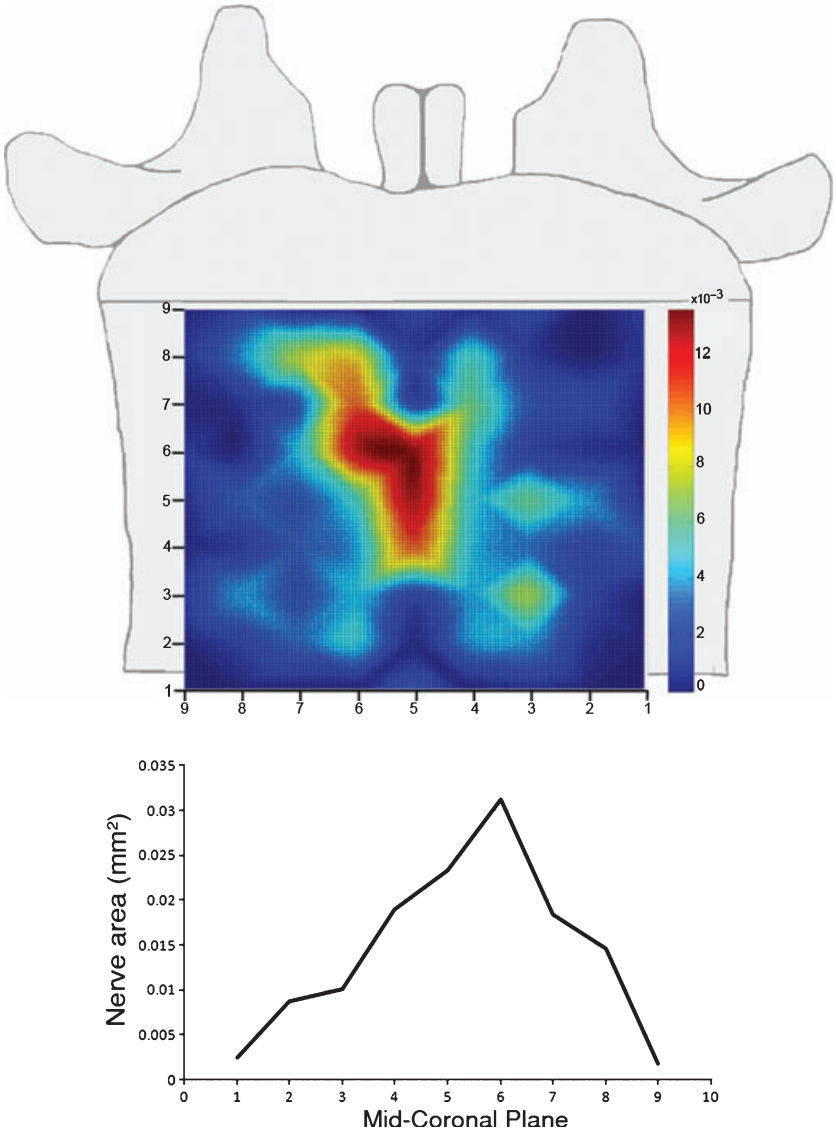

Fig. 7 Top image shows the nerve area (mm^2) distribution averaged across five mid-coronal sections from the L4 specimen. Bottom image is a graph quantifying the nerve area along the equatorial plane of the same five mid-coronal sections, demonstrating the higher quantity of nerve in the center compared to the periphery.

reported that elevated vertebral interosseus pressure can cause pain ((Esses & Moro, 1992), interosseus pressure is increased in low back pain patients (Arnoldi, 1976), and that pain amelioration with vertebroplasty (injection of cement into the vertebral centrum to treat vertebral fractures) may be due to nerve ablation (Niv et al. 2003).

As part of the healing process, there is an increased proliferation of vessels and vertebral capillaries. The vertebral endplate serves as a porous interface with the intervertebral disc through which transport is maintained between intervertebral disc cells and vertebral capillaries. This porosity causes the endplate to be deformable during spinal pressure fluctuations concurrent with the activities of daily living. For example, Heggeness & Doherty (1993) measured endplate deflections in the range of 0.3 mm during disc pressurization of 70–100 psi. Further, the endplate is the weak link during spinal compression and the primary site of vertebral damage accumulation (Adams et al. 2000; Gallagher et al. 2006) that is commonly present in patients with degenerative disc disease (Brown et al. 1997) and low back pain (Freemont et al. 2002). Consequently, if nociceptors arising from the BVF are present at this deformable and damage-prone interface, it may be that some forms of disc pain are actually vertebrogenic.

Histologic techniques are useful for observing the cellular morphology within bone, as the embedding process fixes the physical nature of the tissues and preserves the marrow cavity architecture. However, given that the interosseus nerves are small and present in high density, it was not possible to directly establish connectivity between individual nerves in adjacent sections that were 200 μm apart. Adding additional complexity was the fact that nerves often obliquely cross the plane of cross-section, leading to variability in nerve areal density calculations. Nerve count, on the other hand, is not affected by this and may be a more reliable indicator of innervation patterns. This is because,

regardless of position or size, a single nerve is quantified uniquely, whereas its cross-sectional area will vary. Yet, the high correlation between nerve count and the areal nerve density (Fig. 4) demonstrates this limitation did not significantly affect our observations.

We chose to utilize an L4 due to the high prevalence of disc degeneration at the L4/L5 segment and its consequential role in low back pain. Due to the laborious nature of our histologic approach, it would be impractical to analyze a larger sample of vertebrae in the same manner. As such, our data represent a significant advance as, until now, inferences on vertebral nerve distribution have been based on only a limited number of sections, or sections of isolated bone samples (Antonacci et al. 1998; Buonocore et al. 2010).

Despite these limitations, our data substantiate prior observations that vertebra are richly innervated. Further, we demonstrate that most vertebral nerves enter through the BVF and course along with blood vessels toward the vertebral centrum, then branch toward the endplates. Because of the intimate structural interactions between vertebra and intervertebral discs, these observations suggest that some forms of pain that have been previously attributed to intervertebral discs may actually arise from adjacent vertebra.

Acknowledgements

The authors thank David Lari for his assistance with the MATLAB code. This work was funded by grants from the NIH (R01AR05281) and Relievant Medsystems.

References

Adams MA, Freeman BJ, Morrison HP, et al. (2000) Mechanical initiation of intervertebral disc degeneration. *Spine (Phila Pa 1976)* **25**, 1625–1636.

Antonacci MD, Hanson DS, Leblanc A, et al. (1997) Regional variation in vertebral bone density and trabecular architecture are influenced by osteoarthritic change and osteoporosis. *Spine (Phila Pa 1976)* **22**, 2393–2401; discussion 2401–2.

Antonacci MD, Mody DR, Heggeness MH (1998) Innervation of the human vertebral body: a histologic study. *J Spinal Disord* **11**, 526–531.

Antonacci MD, Mody DR, Rutz K, et al. (2002) A histologic study of fractured human vertebral bodies. *J Spinal Disord Tech* **15**, 118–126.

Arnoldi CC (1976) Intraosseous hypertension. A possible cause of low back pain? *Clin Orthop Relat Res* **115**, 30–34.

Bogduk N (1983) The innervation of the lumbar spine. *Spine (Phila Pa 1976)* **8**, 286–293.

Bogduk N, Tynan W, Wilson AS (1981) The nerve supply to the human lumbar intervertebral discs. *J Anat* **132** (Pt 1), 39–56.

Brown MF, Hukkanen MV, McCarthy ID, et al. (1997) Sensory and sympathetic innervation of the vertebral endplate in patients with degenerative disc disease. *J Bone Joint Surg Br* **79**, 147–153.

Buonocore M, Aloisi AM, Barbieri M, et al. (2010) Vertebral body innervation: implications for pain. *J Cell Physiol* **222**, 488–491.

Crock HV, Yoshizawa H (1976) The blood supply of the lumbar vertebral column. *Clin Orthop Relat Res* **115**, 6–21.

van Dieen JH, Weinans H, Toussaint HM (1999) Fractures of the lumbar vertebral endplate in the etiology of low back pain: a hypothesis on the causative role of spinal compression in aspecific low back pain. *Med Hypotheses* **53**, 246–252.

Esses SI, Moro JK (1992) Intraosseous vertebral body pressures. *Spine (Phila Pa 1976)* **17** (6 Suppl), S155–S159.

Fagan A, Moore R, Vernon Roberts B, et al. (2003) ISSLS prize winner: the innervation of the intervertebral disc: a quantitative analysis. *Spine (Phila Pa 1976)* **28**, 2570–2576.

Freemont AJ, Watkins A, Le Maitre C, et al. (2002) Nerve growth factor expression and innervation of the painful intervertebral disc. *J Pathol* **197**, 286–292.

Gallagher S, Marras WS, Litsky AS, et al. (2006) An exploratory study of loading and morphometric factors associated with specific failure modes in fatigue testing of lumbar motion segments. *Clin Biomech (Bristol, Avon)* **21**, 228–234.

Groen GJ, Baljet B, Drukker J (1990) Nerves and nerve plexuses of the human vertebral column. *Am J Anat* **188**, 282–296.

Heggeness MH, Doherty BJ (1993) Discography causes end plate deflection. *Spine (Phila Pa 1976)* **18**, 1050–1053.

Humzah MD, Soames RW (1988) Human intervertebral disc: structure and function. *Anat Rec* **220**, 337–356.

Kuslich SD, Ulstrom CL, Michael CJ (1991) The tissue origin of low back pain and sciatica: a report of pain response to tissue stimulation during operations on the lumbar spine using local anesthesia. *Orthop Clin North Am* **22**, 181–187.

Mach DB, Rogers SD, Sabino MC, et al. (2002) Origins of skeletal pain: sensory and sympathetic innervation of the mouse femur. *Neuroscience* **113**, 155–166.

Malinsky J (1959) The ontogenetic development of nerve terminations in the intervertebral discs of man. (Histology of intervertebral discs, 11th communication). *Acta Anat (Basel)* **38**, 96–113.

Niv D, Gofeld M, Devor M (2003) Causes of pain in degenerative bone and joint disease: a lesson from vertebroplasty. *Pain* **105**, 387–392.

Ratcliffe JF (1980) The arterial anatomy of the adult human lumbar vertebral body: a microarteriographic study. *J Anat* **131** (Pt 1), 57–79.

Ratcliffe JF (1981) The arterial anatomy of the developing human dorsal and lumbar vertebral body. A microarteriographic study. *J Anat* **133** (Pt 4), 625–638.

Ratcliffe JF (1986) Arterial changes in the human vertebral body associated with aging. The ratios of peripheral to central arteries and arterial coiling. *Spine (Phila Pa 1976)* **11**, 235–240.

Sherman MS (1963) The Nerves of Bone. *J Bone Joint Surg* **45A**, 522–528.

Weishaupt D, Zanetti M, Hodler J, et al. (2001) Painful lumbar disk derangement: relevance of endplate abnormalities at MR imaging. *Radiology* **218**, 420–427.